Distinct Absorption Transducing Features of Silica Supported MoO_3/PANI Hybrid Coated Optical fiber towards Malathion Monitoring in food samples

[1]Z. Heidarnia, [2]R. Parvizi*, [1,3]H. Khoshsima, [4]H. Heidari

[1] *Research Institute for Applied Physics and Astronomy, University of Tabriz, Tabriz 5166616471, Iran*

[2] *Department of Physics, College of Sciences, Yasouj University, Yasouj 75914-353, Iran*

[3] *Faculty of Physics, University of Tabriz, Tabriz 5166616471, Iran*

[4]*Microelectronics Lab, School of Engineering, University of Glasgow, Glasgow G12 8QQ, United Kingdom*

Abstract: This work will show, for the first time, the absorptive silica-supported polyaniline (PANI) molybdenum trioxide (MoO_3) semiconductor hybrid coating onto the optical fiber realizing the concept of lossy mode resonance (LMR) incorporated with molecular imprinting (MIP)-based sensors. The unique optical absorptive and imprinting (IP) properties and possessing a proper refractive index, introducing a versatile optical transducer, were assessed in the detection of Malathion (MAL) to address the rising concern of pesticide residue in crops. The accurate structural and morphological characterization confirmed the rough crystalline and spherical particles for a ternary composite of PANI, SiO_2, and MoO_3 onto an optical fiber curved surface while spectroscopic analysis confirms the formation of imprinting polymer and desirable absorbance characteristics. The experimental and numerical sensing studies revealed that the proposed sensing probe allows the rapid adsorption/desorption of MAL to the sensing films and highly permeable coating under studying the effective parameters influence. The optimized probe exhibits an excellent performance with the maximum sensitivity of within 14-224 µM with the linearity coefficient of R^2= 0.99 possessing a low limit of detection of 9.1 nM. Additionally, this sensor selectively detects. in the presence of other real species and also showed good recovery in the various corps samples.

Keywords: Polyaniline**,** molybdenum trioxide, silica, optical fiber sensor, Malathion.

Introduction

Many efforts have been performed to develop various analytical methods for detection of pesticide residue, such as gas, mass spectrometry, high performance liquid chromatography (HPLC) and gas chromatography (GC) [1, 2], gas chromatography-mass spectrometry (GC-MS) [3],

chemiluminescence [4], and colorimetric sensing [5-8]. Although these common detection techniques of GC, HPLC and GC-MS provide such a high sensitivity and good accuracy, these strategies raise a number of issues related to complexity, cost, and time-consuming. Also, chemiluminescence has the advantages of simple instruments, fast detection, low limits of detection, and wide dynamic range, while suffering from poor selectivity and stability. Among all these analytical methods, colorimetric method incorporating nobel material such as gold nanoparticles (AuNPs) has received great attention owing to its rapidity, high sensitivity, and potential on-site detection ability based on the operating principle of localized surface plasmonic resonance (LSPR) [9]. Despite that LSPR detection methods have been developed for rapid detection of malathion residues with a detection limit down to 0.15 μM and 0.5 pM by exploiting aptamer in water and real samples, respectively reported by Kohzadi et al. Bala et al. reported [10, 11] but these techniques have also varies drawbacks of high costs, eligible operators and complicated instruments, making them not suitable for onsite and real time detection [4, 5, 12].

Recently, visible absorption spectroscopy-based optical fiber sensors have been attracted more consideration for their unique properties such as intrinsic immunity to electromagnetic interference, small size, low cost, high sensitivity to refractive index changes, real time and onsite detection ability, and rapid response and recovery time [6-9, 13-16]. This work presented the use of optical fiber sensor based on lossy mode resonance (LMR) synthesized with a very selective sensing layer for fast MAL detection at low concentrations in which an attenuation at a special wavelength range is observed, which is called LMR. These emergence of resonances are not limited using specific material (e. g. nobel metals) and are feasible by using wide range of materials including semiconductors, dielectric and polymers [9, 17]. Molybdenum trioxide (MoO3) is an n-type semiconductor material with a versatile stoichiometry, changing oxidation situations (+2 to +6), good catalytic acting, wide tunable bandgap (3.1 eV) and well biocompatibility. Due to these unique characteristics, MoO_3 is being applied for wide applications including biomedical sensors [18, 19]. In this work MoO3 thin film has been prepared using a sol-gel path [20, 21] by exploiting the silica network of interlinked pores. Besides rendering the

facility in synthesizing, mechanical stableness, optical clearness and great porosity, the main and important point is that, sol–gel technique at rather low temperatures allows their integration into complex sensor systems [22], herein is adhesion of sensing agents to the optical fiber surface,. Optimization of the thin film parameters through its fabrication lets to create the best efficiency of the sensor in terms of sensitivity. Between these parameters, the layer thickness is highly important [23-26]. These sensors are used as biosensors with extremely low limit of detection [27]. In the next step, as of the important parameters in evaluating sensor performance is selectivity Molecular Imprinted Polymers (MIP) was exploited which is also named "plastic antibodies", is able to specifically recognize and selectively adsorb specific target molecules [28-30]. In practical sensing application, up to our knowledge, the MIP-based have not been performed for optically detection of MAL [31], especially by using polyaniline, (PANI). Owing to unique electrical, electrochemical properties, high environmental stability, easy polymerization and low cost of monomer [32], incorporating PANI with SiO_2/MoO_3 onto optical fiber curved surface introduces a versatile optical absorptive transducer to detect low volume of Mal in the corpse. Since the silica supported MoO3 agents form chemical bonds with molecules containing functional groups of PANI, this leads to different semiconducting properties depending on their nature. This work focuses on design, fabricating and characterizing a versatile MAL fiber-based sensor by coating LMR/MIP responsible functional layers to detect pesticide in aqueous media. These properties represent improvements in water resistance, interfacial adhesion, and optical and electrical properties that have been optimized, as an LMR fiber-based optical sensor.

Experimental

Sensing probe fabrication:

(a) pretreatment of the fiber optic probe

The multimode plastic-clad silica fiber with a core diameter of 400 μm is used in fabrication of the sensor. After removing the outer jacket of a 10cm length of optical fiber, to expose the evanescent field

of core modes, the clad of 1.5 cm length of fiber is etched chemically by immersion of the fiber in a 40% HF solution for 90 min. Before coating the thin film, it is necessary to explore the speed of etching to optimize the leaked light from the etched region (evanescent light) according to the attenuated output power. It means that we have to tradeoff between the leaked light and the transmitted output light intensity. When the etching is more than a critical stage, the fiber become very thin leading to an intensive evanescent wave. On the other hand, it should be noted that the longer etching time causes a very low intensity of transmitted output light leading not able to recognize properly the variations. Therefore, we have etched optical fiber with time of 90 min and the 60% of light can be transmitted through the etched fiber and the output power experiences nearly 40% loss which is a proper intensity of measurement, as reported in our earlier works [17]. Then the unclad-fibers are placed in piranha solution for several hours, which removes resistant organic matter from the silica surface and makes the cleaned surface extremely hydrophilic. Both heads of the fiber are then polished with 2000-gritd polishing film that increase the intensity of the outing light of fiber [33-35]. Fig. 1 (a) and (b) shows schematic and image of optical fiber before and after etching.

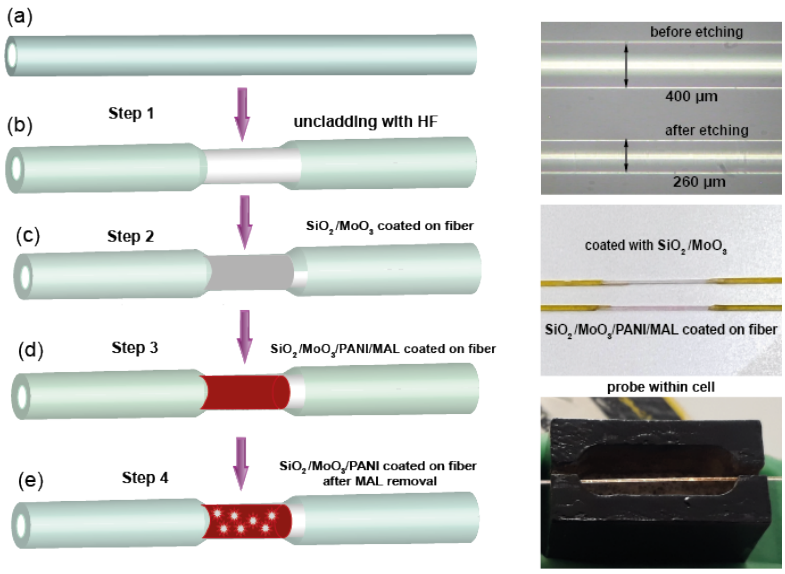

Fig.1. Sensor probe preparation steps along with the images of the undergoing optical fibers.

(b) Synthesis of MoO_3 and silica supported MoO_3 thin films

First, MoO_3 is synthesized by the following method. In a generic synthesis, 2.5 g (0.01 mol) sodium molybdate is solved in 30 ml of instilled water under magnetic stirring. Thereupon 12 ml HBF4 is gently increased into the solution. After 10 min stirring, the obtained solution is transferred and sealed in a Teflon-lined stainless autoclave with a capacity of 100 ml, and the autoclave is heated to 180 °C for 24 h. After the reaction, the autoclave is allowed to cool down to the room temperature naturally. Finally, the precipitate is washed several times with absolute ethanol and distilled water, respectively, and then dried at 60 °C for several hours and kept for further characterization. As a contrast experiment, 1.67 g H2MoO4 (0.01 mol) is dissolved in 30 ml of distilled water and then 12 m HBF4 is gradually added into the solution or not. Finally, the obtained solution is kept at 180 °C for 24 h by a hydrothermal reaction**.**

Then, SiO_2 supported MoO_3 film preparation was carried out using the sol–gel dip-coating method. Solgel is an optically transparent glasslike material formed by hydrolysis and polymerization of metal alkoxides or metalorganic compounds. The silica glass formed by this method is a porous matrix that contains interconnected pores formed by a three-dimensional network of SiO_2. This hydrolysis resulted in the formation of silanol groups (Si–OH) and the silanol groups reacted more to form siloxane polymers (Si–O–Si). First, the solution was prepared by dissolving 1 ml of Tetraethyl orthosilicate (TEOS) and 0.3 ml of (3-Aminopropyl) triethoxysilane (APTES) as Precursor in 10 mL of methanol as solvent. This solution was continuously stirred for 30 minutes without temperature to yield homogeneous solution. Then, added 3 drops of glycine solution (0.01 g of glycine in 10 ml of water) which is a surfactant and causes a thin layer and 0.2 ml diluted HCl (2ml of HCl of 37% in 15 ml of water) as a catalyst to initiate the reaction. After that, again the solution was stirred for 10 min. Subsequently, the MoO_3-doped sol solution was prepared by mixing 5 ml of MoO_3 solution (.01 gr of MoO_3 in 10 ml of ethanol) into the sol solution [36]. Then, optical fibers were placed into the solution

at various intervals and coated. Various ratios of the above substances were tested to we found optimal values to give the best performance. Fig.1 (c) shows fiber coated with SiO2 supported MoO_3 layer.

(c) polymerization: MIP, NIP

Fig. 2 depicts schematic of the synthesis procedure for molecular imprinting polymer on the etched optical fiber; it was obtained by in situ oxidative polymerization of aniline in the presence of an oxidizer ammonium persulphate (APS). In the first step, (Fig. 2), 0.4 mL of aniline (100% in concentration), 3 mL of HCl (0.5 M, 25% in concentration) and 16 mL of ethanol were mixed together and refrigerated for 3 h. Then, 13 mL of APS (0.1 M in 50 mL) and 2 ml of Malathion toxin as an analyte were added to this mixture. Above compound continuously was stirred for 2-8 hr. The polymer produced in this step is called non- molecular imprinting (NIP) because the analyte molecules are still present inside the polymer. Finally, ethanol and DI water were used to wash the solution Which then creates a MIP layer [37]. Fig.1 (d) and (e) show NIP and MIP coated on optical fiber respectively.

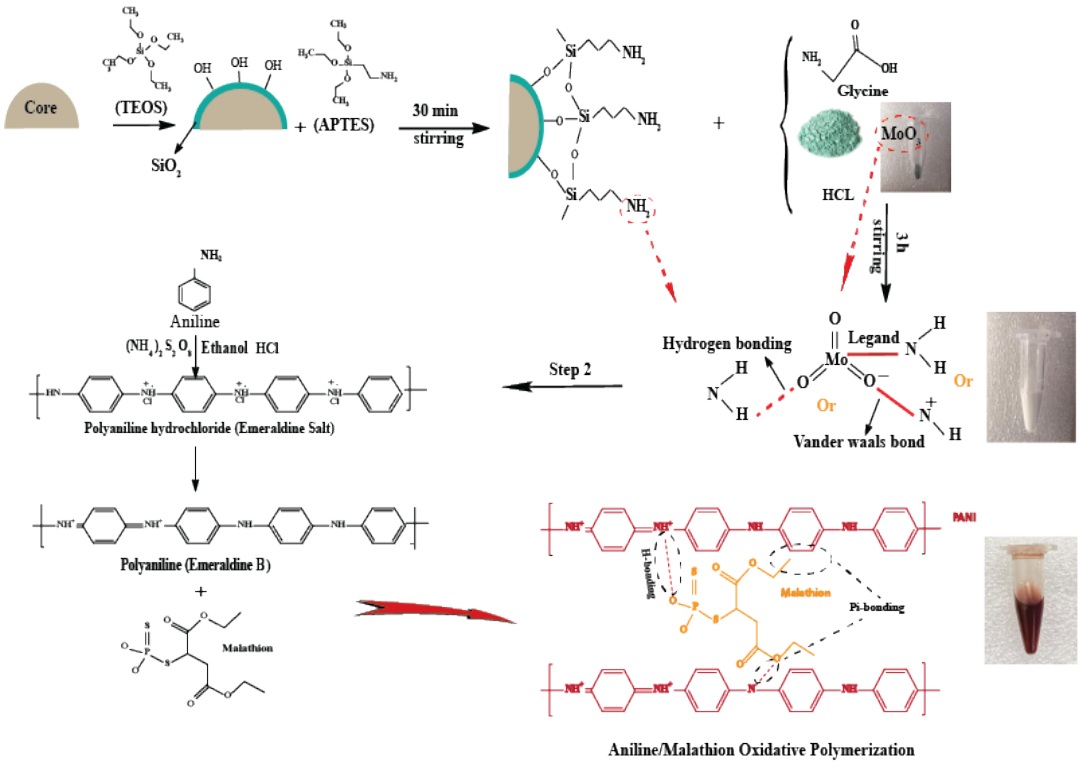

Fig.2. Schematic of the synthesis procedure for molecular imprinting polymer

Determination of Malathion in solution samples

The experimental setup for MAL detection is consist of a white light source (tungsten-halogen lamp) is used for connecting to optical fiber probe that is in contact with the medium that is being investigated. The output end of the fiber is connected to Ocean Optic spectrometer. The data is obtained from signal processing on a laptop. The spectral variation at the fiber output end that is the result of the evanescent wave absorption is then recorded with software from Ocean Optics**.** The optical fiber coated region is embedded inside a cell. The sensitive area of the sensor probe in the cell is exposed to different concentrations of malathion in the range of 300 nM to 1 mM, respectively. Then changes in the output spectrum of the fiber are recorded.

Results and discussion

Characterization

Fig.3 (a) describes the XRD pattern of the MoO_3 in the range, 10−80°. The peaks found at 2θ = 12.8, 23.5, 25.8, 27.4 and 39.1° were displayed to the characteristic hkl planes of MoO_3 at (001), (100), (002), (011) and (003), corresponding to the orthogonal structure of MoO_3 with the lattice parameters (a = 3.95, b = 3.68, and c = 7.09). The highest intensity apperceived at 2θ = 27.44° at the plane (011) manifested that MoO3 crystallites grew more regular along the (011) plan [18]. XRD pattern amorphous SiO_2/MoO_3 are shown in Fig.3 (b). The broad band XRD of SiO_2/MoO_3 at theta = 22.5◦ indicated in Fig. 3 (b). This is in correspondence with same XRD patterns of amorphous silica [38, 39]. Fig.3 (c) illustrates XRD diffraction pattern of polyaniline. This analysis indicates an amorphous structure with a broad peak centered on 2θ ≈ 26.400 [40, 41]. Additionally, the broad peaks of PANI display an amorphous nature of the polymer [40] and the immerged sharp in PANI/MAL/IP correspond to the structure of MAL [42]. Fig. 3 (d) shows the diffraction pattern of PANI/MAL/IP peaks at 2θ: 8.45°,

14.83°, 20.90° and 26.31°. Therefore, incorporation of MAL modifies the structural character of PANI. The FTIR spectra in Fig. 3 (e) display stable interference. The stretching mode of MO-O-MO are located at 989 cm^{-1} and 873 cm^{-1}. The absorption bands at 611 and 481 cm^{-1} are assigned to stretching vibrations of the O(3) and O(2) atoms linked to two or three molybdenum atoms, respectively. The broad band at about 3423 cm^{-1} and the peak at around 1635 cm^{-1} are the O–H stretch and the bending of water [43-46]. FTIR spectra of in Fig. 3 (f) undoubtable confirm the presence of hydroxyl (OH) groups because of absorption bands at 3473, 2927 and 1637 cm^{-1} and absorption band at 1057 cm^{-1} relates with Si–O vibrations. Generally, due to the Mo-O vibration, has created breaded peak and absorption bands below 1000, which are related to O(3) and O(2) stretching vibrations, are almost eliminated [47-49]. Fig. 3 (g) shows FTIR spectroscopy of PANI. The peak at 1450 cm^{-1} is ascribed to a C-N stretching in the proximity of a quinanoid ring. The 1326 cm^{-1} band is appropriated to the C-N stretch of a secondary aromatic amine, because of different configurations of the polymer, the C-N bond has different chemical perimeters, and it leads to different frequencies of the C-N stretching vibration band. In the bands of 1048 and 877 cm^{-1}, respectively the aromatic C-H in-plane and out-plane bending modes are apperceived. O–H stretching vibrations were also observed at 2974 cm^{-1} [50-53]. Fig.3 (i) shows the registered FTIR spectrum for the malathion. The signal at 1731 cm−1 is due to the stretching of carbonyl of the ester group. The absorptions band about 1455 and 1370 cm^{-1} are because of the various vibrational modes of -CH2 and CH3 groups. The band at 1008 cm^{-1} is due to stretching of P-OCH3 group, while the absorption band that visible at 2981 cm^{-1} stems from the alkyl chains [54, 55]. Fig.3 (h) shows FTIR spectra of PANI/MAL/IP. A comparison between Fig. 3(h) and (i) shows that the adsorption band 1731 cm^{-1} created in PANI/MAL/IP is due to the presence of malathion in the PANI.

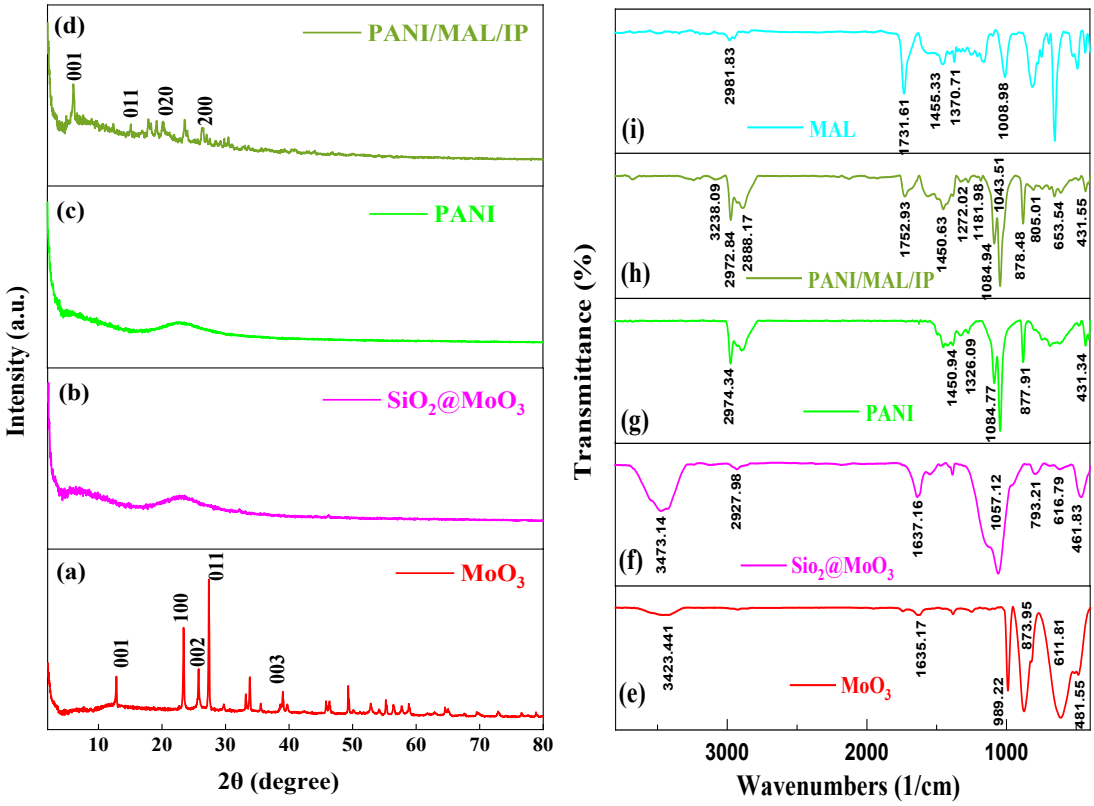

Fig3. X-ray diffraction and FTIR of composites

The morphology of the nanocomposite coatings over optical fiber were verified at each step by the scanning electron microscopy (SEM) images. Figure 4 (a) and (b) illustrates SEM images of surface and cross section of coated optical fiber with silica. After functionalization and coating of SiO_2/MoO_3 surface optical fiber with PANI during nanocomposite, their dispersibility and homogeneity also well deposited as evident from Fig. 4 (c) and (d) SEM images. In Fig. 4(a) and (c) images a homogenous distributed spherical nanoparticles with the mean size of ~30-40 nm with a compact morphology is observed. These results evidence that the polymer was well deposited on the optical fiber surface. Energy dispersive X-ray spectrometry (EDS) analysis results shown in fig.2s.Fig 2S (a) confirm the presence of molybdenum in silica supported MoO_3 layer.

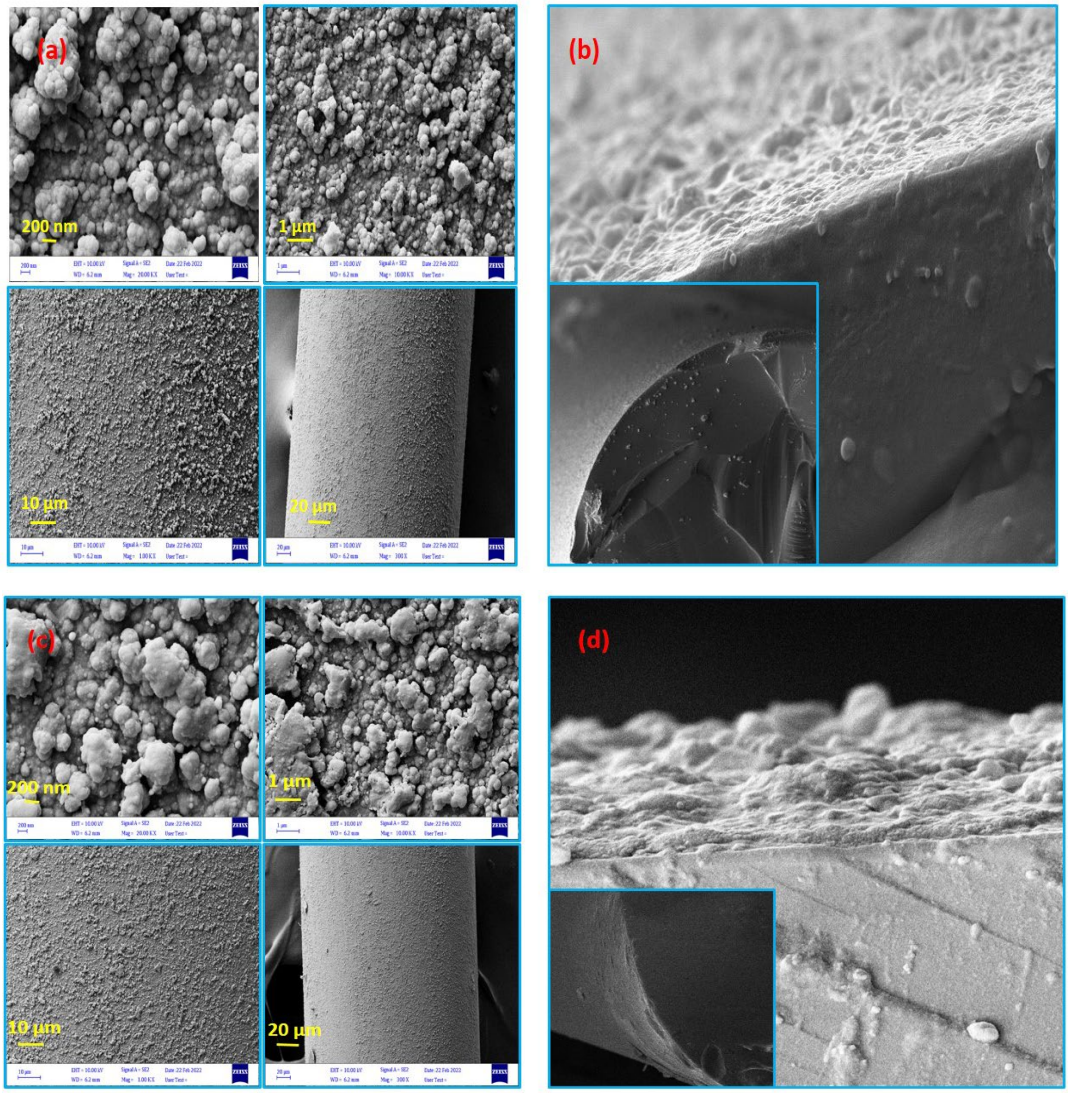

Fig.4 (A) and (B) SEM of surface and cross section of silica supported MoO_3 layer. (c) and (d) SEM of surface and cross section of MIP layer

UV-vis spectroscopy

The optical characteristics of the SiO_2/MoO_3/PANI solution were evaluated by a UV−Vis spectrometer. The SiO_2/MoO_3 nanoparticles could absorb visible light upon PANI incorporation, which resulted from PANI optical absorption of visible light, especially by red color region, Fig. 5. The as-prepared MAL incorporated SiO_2/MoO_3/PANI in an aqueous solution exhibit an intense absorption spectral from 400

to 600 nm; implying the trace of MAL molecules presence clearly by the emergence of stronger absorption within the starting visible region (around 600 nm). This can directly introduce this composite as an efficient and versatile sensing layer to trap and detect MAL molecules.

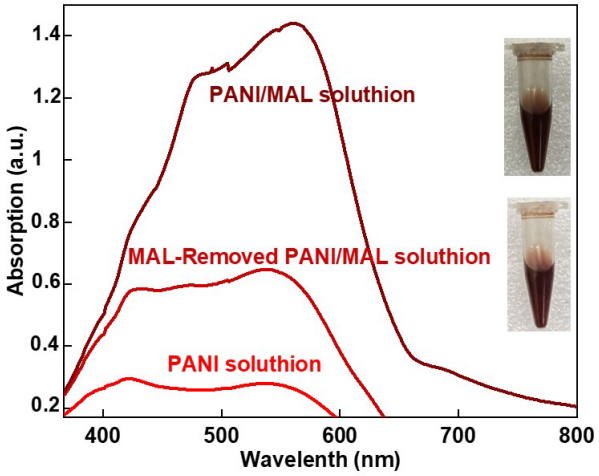

Fig. 5. UV–VIS absorption spectra of sensing solution without analyte (NIP), red color line, MIP solution analyte (MIP-MAL removed), darker red color line, MIP solution including MAL, darkest red color line.

Theory

In order to find out an intuitive understanding of the LMR effect of the as-prepared coated layers, a theoretical study to recognize and characterize the optical absorptive features of the coated optical fiber was also displayed in more details. Herein, to disclose the concrete absorbing sensing mechanism, the finite element method (FEM) with commercial software (COMSOL Multiphysics) was used to analyze the effective refractive index and electric field distribution of the guided modes in the core region. The details of the simulation model and calculated parameters are introduced in our earlier work [17]. The main differential wave equation is solved within the whole structure with considering the continuity and boundary condition as more detailed theory and the main equation was reported in the Appendix of our earlier work [17] with choosing a proper mesh distribution. For this purpose, the etched core at 100 µm diameter is taken as pure silica dielectric with the refractive index of the optical fiber core considered as 1.45 according to the its data sheet. The first coating layer is a silica composite

Eq. (1)

incorporated MoO_3 with about 110 nm thickness whose effective dielectric function of the composite can be calculated from Maxwell-Garnett model given in Eq. (1) [56], as following

$$\varepsilon_{eff} = \varepsilon_2 \frac{\varepsilon_1 + 2\varepsilon_2 + 2f(\varepsilon_1 - \varepsilon_2)}{\varepsilon_1 + 2\varepsilon_2 - f(\varepsilon_1 - \varepsilon_2)}$$

Where for two component materials with dielectric constants, ε_1 (component 1, nanoparticles) and ε_2 (component 2, dielectric host material), and f is the filling fraction of first component (MoO_3) into second component (SiO_2), where was estimated from the volume incorporated into the solution according to the above mentioned experimental procedure. the effective dielectric function of the composite material (SiO_2/MoO_3) was calculated by this formula. Thereby effective refractive index, which is the square root of dielectric constant, for this layer is 1.65. The LMR is very sensitive to the thickness of the integrated SiO_2/MoO_3/PANI ternary composite such that the thickness was considered 170 nm according to the cross-section view of SEM image of the optimized as-prepared probe (Fig. 4 (b and d)) with effective refractive index for this layer also calculated 1.7 from Eq (1). The preliminary numerical assessment was carried out via the electromagnetic frequency domain module for two-dimensional modeling from cross section point of view with considering the light propagation along the optical fiber both in the transverse component and in the z component. Solving the eigenvalues problem is solved of a five layered waveguide structure, i.e. core, SiO_2/MoO_3 composite as first layer, polyaniline with MAL as second layer, surrounding solution and lastly, air layer. In this case the problem is solved as a 2D calculation.

In this calculation, mode analysis technique is used for the fiber whit two layers coating and the normalized electric field and corresponding the z component electric field distribution of several guided core modes were depicted in Fig. 6. The results supported for first modes of this structure which is acting as a waveguide are presented in Fig. 6 (a) and (b), respectively. To better understand the coupling of propagating light of some higher modes into the coating layer resulting lossy modes [57], the electric field core-guided mode distribution was indicated at launched wavelength light of 620 nm, second box

in Fig. 6 (a and b). It can be seen that the electric field distributions of the lossy modes in the vicinity of the coated layer resulting to the strongest coupling between the core guiding modes and leaked modes of coated layer. In this situation, the phases match well, and the energy of emerging higher order modes transfer to the coating layer; implying transit maximally into the lossy mode. The longitudinal point of view also was illustrated as shown in Fig. 6 (c and d). The Eigen-value mode analysis results revealed the electric field distributions in the vicinity of the coated layer resulting to the strongest coupling between the core guiding intensity and leaked intensities of coated layer. The decaying behavior of evanescent field along the fiber longitudinal could be observed clearly such that the norm of electric field and the z component in a magnified scaled were confined in the interface facet allows the evanescent wave trapping in this region, leading to the sensing enhancement.

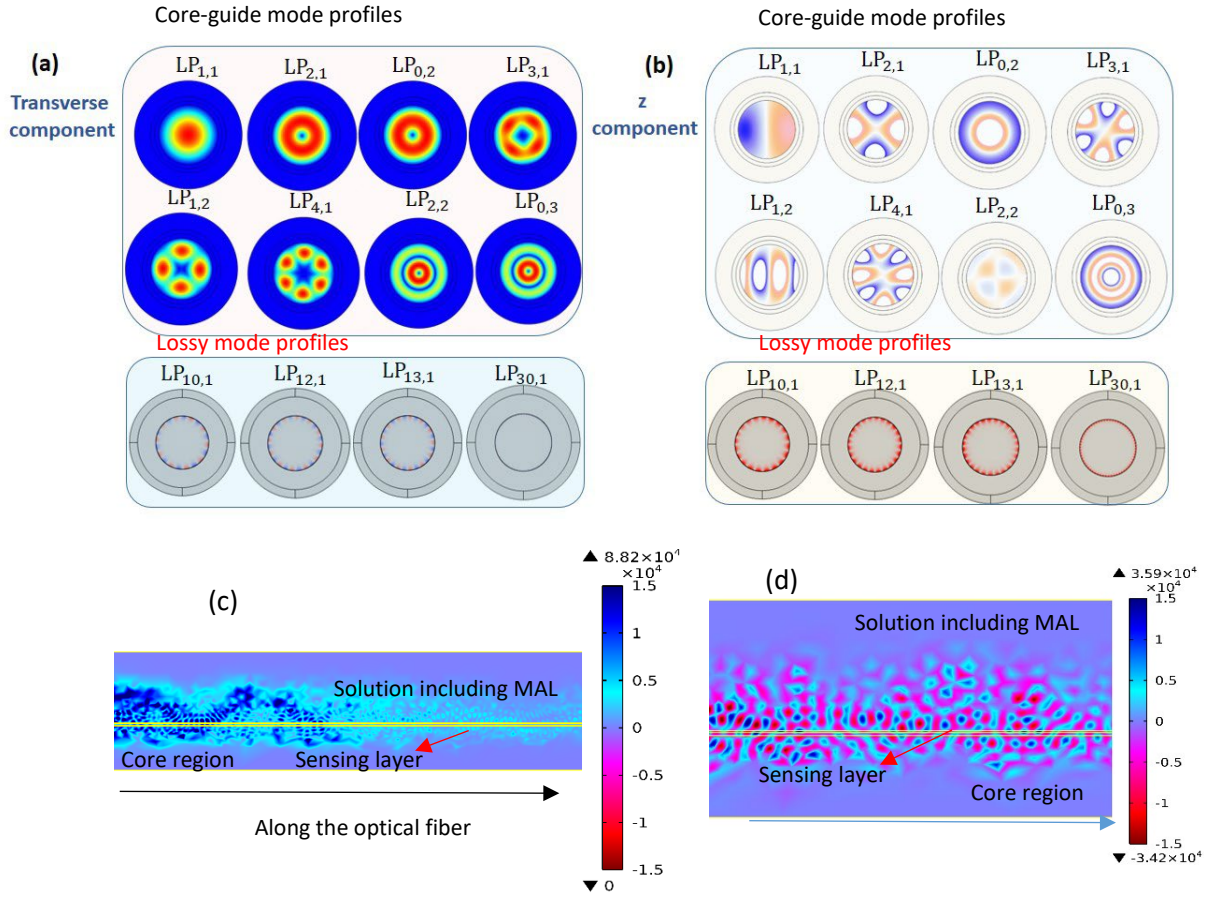

Fig. 6 (A) Mode profile of norm of E (left side) and the corresponding z components (right side) of core-guided and lossy modes of ternary composite SiO_2/MoO_3 and PANI bilayer coated on optical fibers, from both views of the cross section and along the optical fiber.

Optimization of sensor probe characterization based on LMR-MIP bilayer coating

To achieve the best sensor performance, first the amount of the main elements in the composition of silica and polymer, namely molybdenum and aniline, were changed to obtain the optimal value (Fig. S1). Then, the thickness of the layers was optimized by changing the synthesis time. Measurement and detection of malathion began at a greater thickness, where the fiber optic probe was in situ for 5 hours in the sol-gel process and 8 hours in the polymerization then were exposed to different concentrations of malathion in the cell in the range of 300 nM to 1000 μM. For each concentration of MAL, we fill up the flow cell with MAL solution, and wait for about 12 seconds to a nearly stable condition to ensure the fully interaction of MAL molecules with MIP layer. As shown in Fig. 7 (a), the transmitted spectra were recorded showing the dip absorption wavelength and intensity values corresponding to the various concentration. After every measurement, deionized water was injected into the flow cell to wash and also to flush away the unbounded or adsorbed analyte molecules. Fig. 7 (b) demonstrates the magnified normalized transmission spectra corresponding to the transmitted spectrum, with various MAL concentration to more clarify the minimum (dip) wavelength changes. A redshift from 579 to 614 nm in dip wavelength has been observed for various MAL concentration which confirms an increase in the real part of the effective refractive index of sensing region. Furthermore, the decrease of transmission minimum value in the same range indicates an increase in the imaginary part of the effective refractive index, as well. As shown in calibration graph, Fig. 7 (c) indicates a linearly decrement of transmission dip and increasing resonant wavelength with linearity coefficient of R-square of about 0.99 and then, gradually saturated versus concentration more than 214 μM which are adopted with sensing performance.

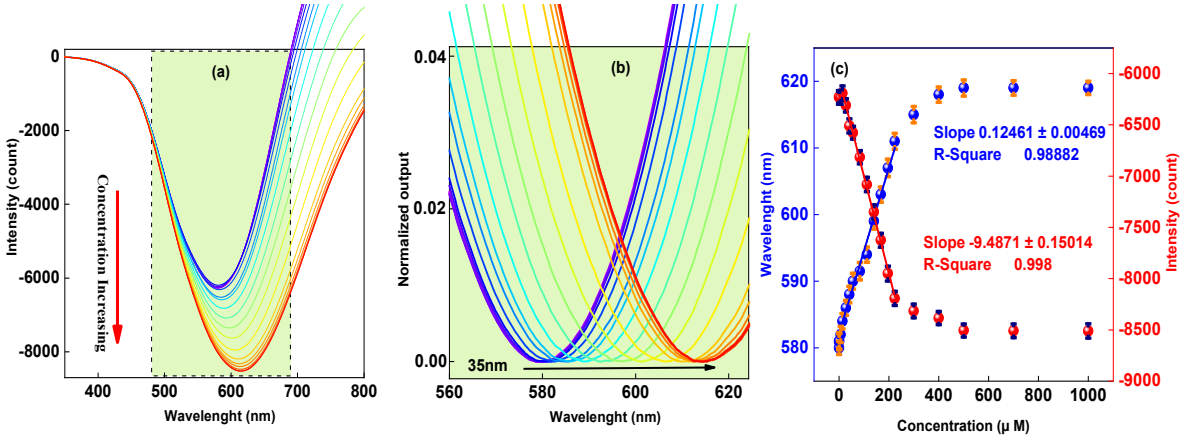

Fig. 7. (a) LMR absorption spectrum of sensing probe coated by SiO_2@MoO_3 with 5 h synthesis time and then undergoes 8 h PANI/MAL polymerization, (b) the magnified normalized transmission spectra indicating 35 nm shift of resonant dip, (c) Calibration curve of LMR absorption spectra.

The exposing synthesis period of every coating layer decides the thickness of the functional layer in a way that directly affect the sensing performance. Herein, the functional layer comprises a LMR responsible layer of silica supported MoO3 layer and a MIP-PANI layer for selective detection of MAL in aqueous environment. The thickness was manipulated by the dipping period of every layer synthesis process to tune and enhance the resonant property. Since the evanescent field decays as the thickness of functionalization layer increases, both LMR and MIP layers thickness according to the synthesis dipping period were changes to find out the optimized sensing performance. Thus, in the following, probes coated with two categories of thin and thinner layers; firstly, only one-layer thickness reduced and then thicknesses of both layers simultaneously reduced and the output spectra were characterized in both wavelength and intensity interrogations. The synthesized conditions of 3 hr SiO_2/MoO_3 and then 8hr PANI/MAL polymerization period was investigated and the results were recorded as shown in Fig. 8 (a, b and c). This SiO_2/MoO_3-LMR layer which is thinner than the as-mentioned prepared probe reported in Fig. 7, with the identical MIP layer, revealed an improved sensing performance in which the dip resonance undergoes a redshift of about 80 nm and linearity coefficient of 0.9955. This

enhancement is attributed to this fact that this thinner LMR can provide more exposed evanescent filed within sensing region. Although, for the case with the thinner MIP-layer prepared with 3hr polymerization synthesis coated on the LMR thickness of 5hr dipping period, the results showed 70 nm redshift of dip wavelength and appreciable linearity. It can be concluded that the reducing LMR thickness was more efficient; emphasizing the significance of LMR role in the proposed sensing performance. In the all sensing studies, the intensity variations were corresponding to the wavelength shifts, so the foundations show identical explanation in terms of intensity interrogation.

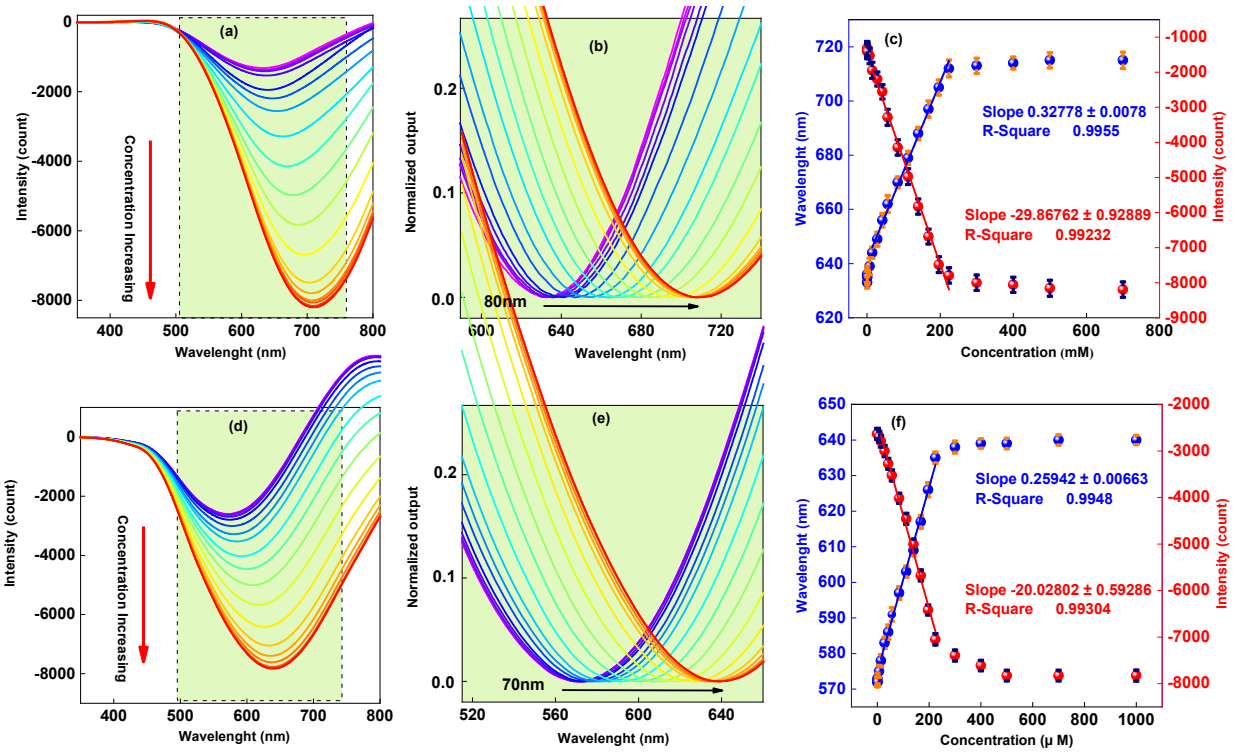

Fig. 8. (a, b and calibration curve, c) LMR- sensing spectra of functional layer synthesized with 3 hr SiO_2 /MoO_3 plus 8 hr PANI/MAL, and (d, e and calibration curve f) LMR–sensing spectra of probe coated with 5 hr SiO_2 /MoO_3 plus 3 hr PANI/MAL synthesized layer.

To further assessment, in the same way, the thicknesses of both LMR and MIP responsible layers were more reduced to 2 hr SiO_2 /MoO_3 along with 3 hr PANI/MAL, and then 3 hr SiO_2 /MoO_3 with 2 hr PANI/MAL synthesized layer. As shown in Fig. 9, probes with the as-prepared functional layers shows nearly similar results without a profound effect on the sensing output rather than above-mentioned conditions, besides that during the measurements, the response time were slightly increased and it needs to wait more to reach a stable condition to record the result.

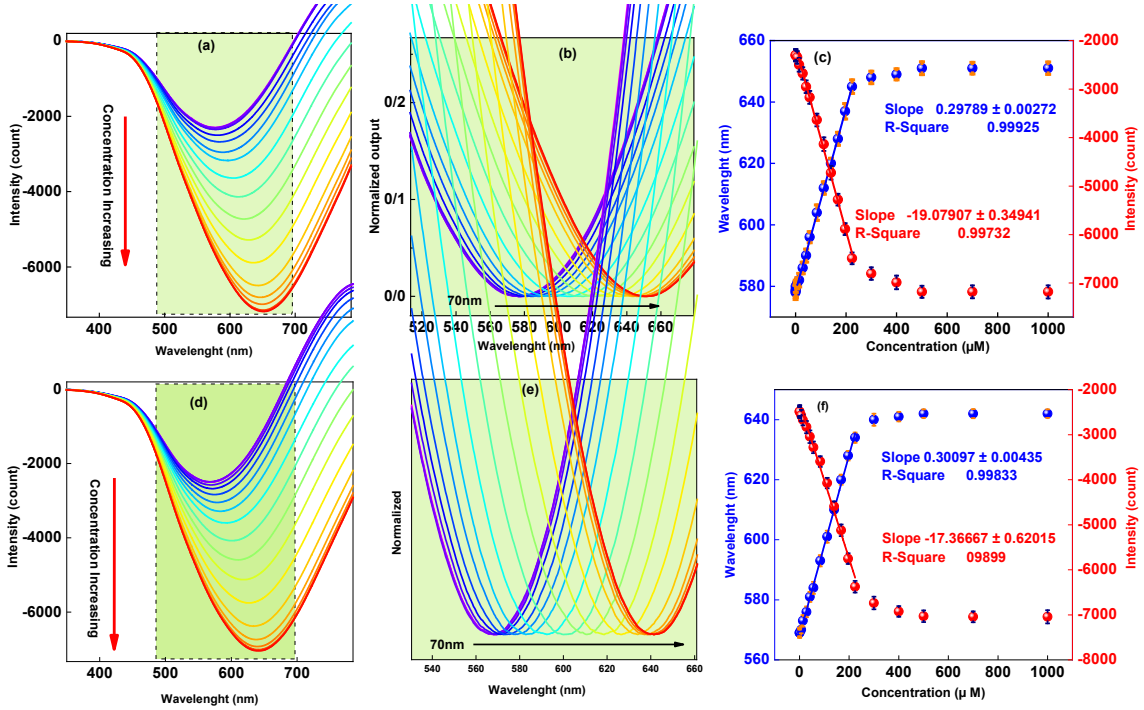

Fig. 9. (a, b and calibration curve, c) LMR- sensing spectra of functional layer synthesized with 2 hr SiO_2 /MoO_3 plus 3 hr PANI/MAL, and (d, e and calibration curve f) LMR–sensing spectra of probe coated with 3 hr SiO_2 /MoO_3 plus 2 hr PANI/MAL synthesized layer.

According to the mentioned results, the best performance of the sensor in terms of wavelength changes and selectivity is related to the fiber optic probe, which has been in the sol-gel process for SiO_2/MoO_3 with 5h synthesis time and then undergoes 8h PANI/MAL polymerization. The rest of sensing studies were carried out by the optimized fiber optic sensing probe. To observe the stability and the response

time of the of the output spectrum of the sensor, the dynamic behavior of the sensor was investigated. Fig. 10 (a) shows the dynamic diagram of sensor under injection of a fixed concentration with several repetitions and Fig. 10 (b) shows the dynamic diagram of sensor against different concentrations, in sequence. The sensor has indicated that the changes in intensity and wavelength, accuracy and response time of the sensor, ignoring a slight difference, are comparable and similar to the results of the first test.

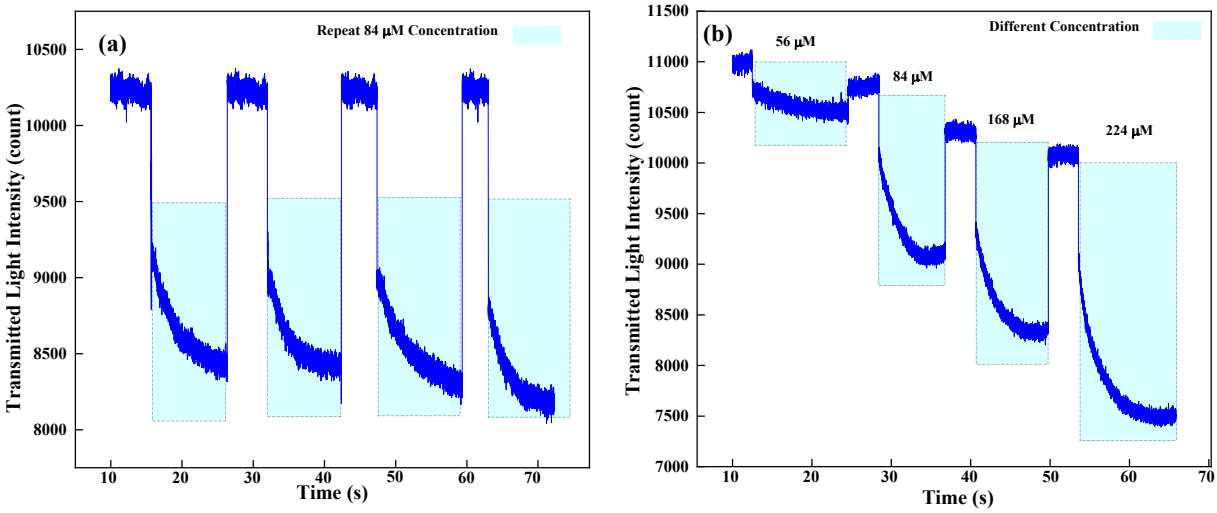

Fig.10. dynamic diagram of sensor (a) under injection of a fixed concentration with several repetitions and (b) against different concentrations, in sequence.

Selectivity and the effect of some interfering species

In order to demonstrate the selectivity of the MIP, various pesticides with equal concentration with MAL concentration (112µM) were injected into the cell and the sensor responses for theses competing molecules were compared with the responses for template analytes. The imprinting factor (IF), that represents the ratio of the sensor response in attendance of MIP probe to NIP probe (IF = MIP/NIP), was investigated for appraisal of imprinting operation (Figure 11(a)). As seen IF factor for malathion is

more than other toxins which illustrate the great selectivity of this sensor. The sensor response for other molecules was considerably low. Also sensor probe with NIP coated did not distinguish between malathion and other pesticides. This high selectivity of the system shows that the MIP method is highly selective for own templates and can does successfully in the sensors for label free selective detection of analyte. A certain concentration of malathion solution was combined with a defined amount of cklorpyrifos, cypermethrin, imidacloprid, propiconazol and fevalerate pesticides widely used in agriculture fields and examined. The results displayed that the existence of other toxins did not effect in MAL detection in this method as the changes in MAL detection was less than 5%. All these results prove the high selectivity of sensor probe towards malathion and negligible detection of other pesticides (Fig. 11 (b)) .

The unique sensitive and selective properties of the proposed sensor may be caused by two factors. First, polyaniline incorporated with MoO_3 in a network was formed by numerous of MoO_3/PANI hybrids as a versatile molecular imprinting which will be favorable to adsorption and diffusion of analyte molecules on the sensing surface. This effect can be attributed to the strong interaction between PANI and MAL molecules driven by strong H-bonding and pi-bonding as shown in Fig. 2. The more important factor being responsible for the enhancement of sensing response is the formation of ternary composite of SiO_2, MoO_3, and PANI as a semiconductor material can absorb the visible light launched through the fiber optic, shown in fig. UV. The formation of p-n heterojunctions at interface between p-type SiO2/MoO3 and n-type PANI [58] with mutual charge transfer until equilibrium being established and making the Fermi level equal in n and p regions [59]. The formation of p–n heterojunctions lowers the activation energy and also provides higher conductivity which is responsible for promoting sensing performance. Nearby the heterointerface of -MoO3 and PANI, the adsorption of MAL results in an increase of the electron concentration in -MoO3, which breaks the original equilibrium and induces a decrease of the width of depletion layer between PANI and -MoO3, leading to further charge transfer

around the junction region and so, the decreasing of the band gap of the sensing layer will emerged as transmitted dip in a longer wavelength position.

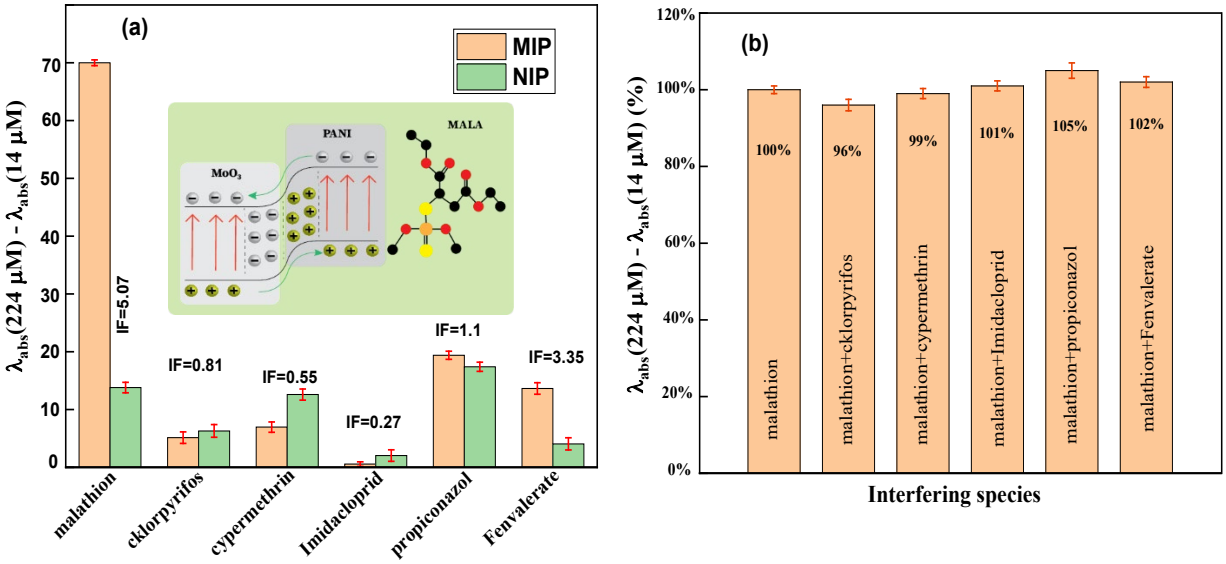

Fig. 11. selectivity of sensor for PANI/MAL/MIP and PANI/MAL/NIP, (b) The effect of some interfering species on determination of MAL

LOD was calculated based on the standard deviation of the response (Sy) of the curve and the slope of the calibration curve (S) at levels approximating the LOD according to the formula: LOD = 3.3(Sy/S). LOD of 9.1 nM has been obtained for this biosensor (Table 1).

Table1. Comparison of the suggested method with the previous reported methods for MAL determination.

Technique Followed	LOD	Refs.
LMR	9.1 nM	Current work
Electrochemical	0.2 µM	[4]
Fluorescence	0.92 µM	[60]
Electrochemical	1 nM	[61]
Raman Scattering	10 µM	[62]
UV-Vis Spectroscopy	2.4 nM	[63]
Amperometric	3.3 nM	[64]

Real sample

To verify the applicability and reliability of sensor, the proposed optimal method was applied to detect malathion in different vegetables juices including lettuce, cucumber and potato. For this, certain concentrations of MAL added to vegetables juices and after applying the method the amount of malathion in vegetable juice was obtained from the graph. Table 4 shows, the relative standard deviation (RSD%) values and recovery. These results demonstrate the usability of senor for practical applications.

Table2. Determination of MAL in vegetable extracts

Sample	MAL added(µM)	MAL found(µM)	Recovery(%)	RSD(%)
Cucumber	112	116	103.6	3.5
	140	137	97.8	2.1
	168	159	94.6	5.3
Lettuce	112	108	96.4	3.6
	140	148	105.7	5.6
	168	173	102.9	2.9
Potato	112	104	92.8	7.2
	140	147	105	4.9
	168	161	95.8	4.1

Conclusion

In conclusion, we demonstrate a silica supported MoO3/PANI sensing film coated optical fiber as a proof-of-concept of hybrid semiconductor and polymer absorptive lossy waveguide selective biosensor. We prove by numerical analysis and experimental measurement that aniline polymeric layer added on a LMR supported film effectively enhances the leaked lossy modes towards transducing the presence of specific analyte molecule demonstrated in both wavelength and intensity interrogations. The fabrication and characterization of the proposed fiber optic sensor were carried out and the optimal constructing condition was determined based on the experimental sensing performance assessments for each as-prepared probe addressing the MAL detection. The sensing probe with the SiO_2/MoO_3 with 5 h synthesis time and then undergoes 8 h PANI/MAL polymerization showed the best sensing results of an appreciable linearity in the concentration range of 14 μM to 224 μM with limit of detection of 9.1 nM. Hence, this optical sensor can be used successfully to determine MAL and introduce optical fiber substrate design as feasible and remote monitoring with required miniaturization for any bio-sensor applications. Additionally, these efficient achievements confirm the label-free diagnosis of Ep, introduce a proposing route to recognize any other specific pesticide, and open up a novel opportunity to quantitatively monitor analyte molecules with a poor concentration in different aqueous matrices.

Reference

[1] P. T. K. Hong and C.-H. Jang, "Sensitive and label-free liquid crystal-based optical sensor for the detection of malathion," *Analytical biochemistry,* vol. 593, p. 113589, 2020.

[2] G. Xu, J. Hou, Y. Zhao, J. Bao, M. Yang, H. Fa*, et al.*, "Dual-signal aptamer sensor based on polydopamine-gold nanoparticles and exonuclease I for ultrasensitive malathion detection," *Sensors and Actuators B: Chemical,* vol. 287, pp. 428-436, 2019.

[3] F. Faghiri, M. Hajjami, and F. Ghorbani, "Development of a sensing system based on coupling magnetic solid phase extraction and colorimetric detection for determination of

organophosphorus pesticides in fruit extract and environmental sample," *Sensors and Actuators B: Chemical,* vol. 343, p. 130157, 2021.

[4] S. Ebrahim, R. El-Raey, A. Hefnawy, H. Ibrahim, M. Soliman, and T. M. Abdel-Fattah, "Electrochemical sensor based on polyaniline nanofibers/single wall carbon nanotubes composite for detection of malathion," *Synthetic Metals,* vol. 190, pp. 13-19, 2014.

[5] G. A. T. Battad, J. G. Estacio, J. L. C. Indiongco, and M. L. Mopon Jr, "Development of a CuFe2O4-reduced graphene oxide-based electrochemical sensor for malathion," in *Key Engineering Materials*, 2020, pp. 41-47.

[6] A. Aziz, H. Lim, S. Girei, M. Yaacob, M. Mahdi, N. Huang*, et al.*, "Silver/graphene nanocomposite-modified optical fiber sensor platform for ethanol detection in water medium," *Sensors and Actuators B: Chemical,* vol. 206, pp. 119-125, 2015.

[7] Ghahrizjani, Reza Taheri, et al. "ZnO–SrAl2O4: Eu Nanocomposite-Based Optical Sensors for Luminescence Thermometry." ACS Applied Nano Materials 4.9 (2021): 9190-9199.

[8] P. Zubiate, C. Zamarreño, P. Sánchez, I. Matias, and F. Arregui, "High sensitive and selective C-reactive protein detection by means of lossy mode resonance based optical fiber devices," *Biosensors and Bioelectronics,* vol. 93, pp. 176-181, 2017.

[9] Q. Wang and W.-M. Zhao, "A comprehensive review of lossy mode resonance-based fiber optic sensors," *Optics and Lasers in Engineering,* vol. 100, pp. 47-60, 2018.

[10] M. Roushani, S. Kohzadi, S. Haghjoo, and A. Azadbakht, "Dual detection of Malation and Hg (II) by fluorescence switching of graphene quantum dots," *Environmental nanotechnology, monitoring & management,* vol. 10, pp. 308-313, 2018.

[11] Lin, Ming, et al. "Polyelectrolyte-Enhanced Localized Surface Plasmon Resonance Optical Fiber Sensors: Properties Interrogation and Bioapplication." ACS Applied Nano Materials (2022).

[12] X. Lu, L. Tao, Y. Li, H. Huang, and F. Gao, "A highly sensitive electrochemical platform based on the bimetallic Pd@ Au nanowires network for organophosphorus pesticides detection," *Sensors and Actuators B: Chemical,* vol. 284, pp. 103-109, 2019.

[13] Ahmed, Israr, et al. "Nanostructured Photonic Hydrogels for Real-Time Alcohol Detection." *ACS Applied Nano Materials* (2022).

[14] A. Socorro, I. Del Villar, J. Corres, F. Arregui, and I. Matias, "Sensitivity enhancement in a multimode interference-based SMS fibre structure coated with a thin-film: Theoretical and experimental study," *Sensors and Actuators B: Chemical,* vol. 190, pp. 363-369, 2014.

[15] O. Fuentes Lorenzo, I. Del Villar, J. M. Corres Sanz, and I. Matías Maestro, "Lossy mode resonance sensors based on lateral light incidence in nanocoated planar waveguides," *Scientific Reports,(2019), 9, 8882,* 2019.

[16] Pathak, Anisha, and Banshi D. Gupta. "Fiber-optic plasmonic sensor utilizing CTAB-functionalized ZnO nanoparticle-decorated carbon nanotubes on silver films for the detection of catechol in wastewater." ACS Applied Nano Materials 3.3 (2020): 2582-2593.

[17] Z. Heidarnia, H. Khoshsima, R. Parvizi, and H. Heidari, "Comprehensive investigation on chalcogenide thin film coated multimode optical fiber: Visible evanescent-wave absorption refractometer," *Journal of Non-Crystalline Solids,* vol. 586, p. 121567, 2022.

[18] S. Augustine, P. Kumar, and B. D. Malhotra, "Amine-functionalized MoO3@ RGO nanohybrid-based biosensor for breast cancer detection," *ACS Applied Bio Materials,* vol. 2, pp. 5366-5378, 2019.

[19] D. Kwak, M. Wang, K. J. Koski, L. Zhang, H. Sokol, R. Maric*, et al.*, "Molybdenum trioxide (α-MoO3) nanoribbons for ultrasensitive ammonia (NH3) gas detection: integrated

experimental and density functional theory simulation studies," *ACS applied materials & interfaces,* vol. 11, pp. 10697-10706, 2019.
[20] S. Jiebing, X. Rui, W. Shimin, T. Wufeng, T. Hua, and S. Jing, "Preparation and characterization of molybdenum oxide thin films by sol-gel process," *Journal of sol-gel science and technology,* vol. 27, pp. 315-319, 2003.
[21] J. Yu, H. Zheng, D. Hou, J. Zhang, and W. Xu, "Silane Coupling Agent Modification Treatment to Improve the Properties of Rubber–Cement Composites," *ACS Sustainable Chemistry & Engineering,* vol. 9, pp. 12899-12911, 2021.
[22] J. Yuk and T. Troczynski, "Sol–gel BaTiO3 thin film for humidity sensors," *Sensors and Actuators B: Chemical,* vol. 94, pp. 290-293, 2003.
[23] A. Ozcariz, M. Dominik, M. Smietana, C. Zamarreño, I. Del Villar, and F. Arregui, "Lossy mode resonance optical sensors based on indium-gallium-zinc oxide thin film," *Sensors and Actuators A: Physical,* vol. 290, pp. 20-27, 2019.
[24] M. Hernaez, B. Acevedo, A. G. Mayes, and S. Melendi-Espina, "High-performance optical fiber humidity sensor based on lossy mode resonance using a nanostructured polyethylenimine and graphene oxide coating," *Sensors and Actuators B: Chemical,* vol. 286, pp. 408-414, 2019.
[25] A. Vicente, D. Santano, P. Zubiate, A. Urrutia, I. Del Villar, and C. R. Zamarreño, "Lossy mode resonance sensors based on nanocoated multimode-coreless-multimode fibre," *Sensors and Actuators B: Chemical,* vol. 304, p. 126955, 2020.
[26] P. Niedziałkowski, W. Białobrzeska, D. Burnat, P. Sezemsky, V. Stranak, H. Wulff*, et al.*, "Electrochemical performance of indium-tin-oxide-coated lossy-mode resonance optical fiber sensor," *Sensors and Actuators B: Chemical,* vol. 301, p. 127043, 2019.
[27] D. L. Bohorquez, I. Del Villar, J. M. Corres, and I. R. Matias, "Generation of lossy mode resonances in a broadband range with multilayer coated coverslips optimized for humidity sensing," *Sensors and Actuators B: Chemical,* vol. 325, p. 128795, 2020.
[28] Z. Liu, Y. Zhang, J. Feng, Q. Han, and Q. Wei, "Ni (OH) 2 nanoarrays based molecularly imprinted polymer electrochemical sensor for sensitive detection of sulfapyridine," *Sensors and Actuators B: Chemical,* vol. 287, pp. 551-556, 2019.
[29] J. W. Lowdon, H. Diliën, P. Singla, M. Peeters, T. J. Cleij, B. van Grinsven*, et al.*, "MIPs for commercial application in low-cost sensors and assays–An overview of the current status quo," *Sensors and Actuators B: Chemical,* p. 128973, 2020.
[30] Kumar, Vanish, and Ki-Hyun Kim. "Use of molecular imprinted polymers as sensitive/selective luminescent sensing probes for pesticides/herbicides in water and food samples." Environmental Pollution (2022): 118824.
[31] Y. Aghoutane, A. Diouf, L. Österlund, B. Bouchikhi, and N. El Bari, "Development of a molecularly imprinted polymer electrochemical sensor and its application for sensitive detection and determination of malathion in olive fruits and oils," *Bioelectrochemistry,* vol. 132, p. 107404, 2020.
[32] G. W. Coates and Y. D. Getzler, "Chemical recycling to monomer for an ideal, circular polymer economy," *Nature Reviews Materials,* vol. 5, pp. 501-516, 2020.
[33] M. R. Lamont, C. M. de Sterke, and B. J. Eggleton, "Dispersion engineering of highly nonlinear As 2 S 3 waveguides for parametric gain and wavelength conversion," *Optics express,* vol. 15, pp. 9458-9463, 2007.
[34] S. Azad, E. Sadeghi, R. Parvizi, A. Mazaheri, and M. Yousefi, "Sensitivity optimization of ZnO clad-modified optical fiber humidity sensor by means of tuning the optical fiber waist diameter," *Optics & Laser Technology,* vol. 90, pp. 96-101, 2017.

[35] Z. Ashkavand, E. Sadeghi, R. Parvizi, and M. Zare, "Developed Low-Temperature Anionic 2H-MoS2/Au Sensing Layer Coated Optical Fiber Gas Sensor," *ACS Applied Materials & Interfaces,* vol. 12, pp. 34283-34296, 2020.

[36] B. Ramezanzadeh, E. Raeisi, and M. Mahdavian, "Studying various mixtures of 3-aminopropyltriethoxysilane (APS) and tetraethylorthosilicate (TEOS) silanes on the corrosion resistance of mild steel and adhesion properties of epoxy coating," *International Journal of Adhesion and Adhesives,* vol. 63, pp. 166-176, 2015.

[37] S. Saha, N. Chaudhary, H. Mittal, G. Gupta, and M. Khanuja, "Inorganic–organic nanohybrid of MoS 2-PANI for advanced photocatalytic application," *International Nano Letters,* vol. 9, pp. 127-139, 2019.

[38] P. E. Imoisili, K. O. Ukoba, and T.-C. Jen, "Synthesis and characterization of amorphous mesoporous silica from palm kernel shell ash," *boletín de la sociedad española de cerámica y vidrio,* vol. 59, pp. 159-164, 2020.

[39] N. Ikladious, N. Shukry, S. El-Kalyoubi, J. Asaad, S. Mansour, S. Tawfik*, et al.*, "Eco-friendly composites based on peanut shell powder/unsaturated polyester resin," *Proceedings of the Institution of Mechanical Engineers, Part L: Journal of Materials: Design and Applications,* vol. 233, pp. 955-964, 2019.

[40] C. Manjula and S. Kalyane, "SYNTHESIS, CHARACTERIZATION AND MICROWAVE ABSORPTION STUDIES OF POLYANILINE-MoO3 COMPOSITES."

[41] S. Sambaza, A. Maity, and K. Pillay, "Enhanced degradation of BPA in water by PANI supported Ag/TiO2 nanocomposite under UV and visible light," *Journal of Environmental Chemical Engineering,* vol. 7, p. 102880, 2019.

[42] M. H. Dehghani, A. H. Hassani, R. R. Karri, B. Younesi, M. Shayeghi, M. Salari*, et al.*, "Process optimization and enhancement of pesticide adsorption by porous adsorbents by regression analysis and parametric modelling," *Scientific reports,* vol. 11, pp. 1-15, 2021.

[43] T. Hirata, "In-situ observation of Mo-O stretching vibrations during the reduction of MoO3 with hydrogen by diffuse reflectance FTIR spectroscopy," *Applied surface science,* vol. 40, pp. 179-181, 1989.

[44] L. Q. Mai, B. Hu, W. Chen, Y. Qi, C. Lao, R. Yang*, et al.*, "Lithiated MoO3 nanobelts with greatly improved performance for lithium batteries," *Advanced Materials,* vol. 19, pp. 3712-3716, 2007.

[45] S. Rakass, H. Oudghiri Hassani, M. Abboudi, F. Kooli, A. Mohmoud, A. Aljuhani*, et al.*, "Molybdenum trioxide: efficient nanosorbent for removal of methylene blue dye from aqueous solutions," *Molecules,* vol. 23, p. 2295, 2018.

[46] Z. Li, L. Gao, and S. Zheng, "SEM, XPS, and FTIR studies of MoO3 dispersion on mesoporous silicate MCM-41 by calcination," *Materials Letters,* vol. 57, pp. 4605-4610, 2003.

[47] M. Komethi, I. Hanafi, and O. Nandras, "Biodegradation, morphological, and FTIR study of rattan powder-filled natural rubber composites as a function of filler loading and silane coupling agent," *Bioresources,* vol. 7, pp. 957-971, 2012.

[48] A. Demšar, B. Colarič, S. Rus, J. Lindav, F. Švegelj, B. Orel*, et al.*, "FTIR spectroscopy and AES study of water containment in SiO2 thin films," *Thin solid films,* vol. 281, pp. 409-411, 1996.

[49] M. Öhman and D. Persson, "ATR-FTIR Kretschmann spectroscopy for interfacial studies of a hidden aluminum surface coated with a silane film and epoxy I. Characterization by IRRAS and ATR-FTIR," *Surface and interface analysis,* vol. 44, pp. 133-143, 2012.

[50] I. Šeděnková, M. Trchova, and J. Stejskal, "Thermal degradation of polyaniline films prepared in solutions of strong and weak acids and in water–FTIR and Raman spectroscopic studies," *Polymer Degradation and Stability,* vol. 93, pp. 2147-2157, 2008.

[51] Z. Ping, H. Neugebauer, J. Theiner, and A. Neckel, "Protonation and electrochemical redox doping processes of polyaniline in aqueous solutions: Investigations using in situ FTIR-ATR spectroscopy and a new doping system," *Journal of the Chemical Society, Faraday Transactions,* vol. 93, pp. 121-129, 1997.

[52] M. Trchová, I. Šeděnková, E. Tobolková, and J. Stejskal, "FTIR spectroscopic and conductivity study of the thermal degradation of polyaniline films," *Polymer Degradation and Stability,* vol. 86, pp. 179-185, 2004.

[53] M. Trchová, I. Šeděnková, and J. Stejskal, "In-situ polymerized polyaniline films 6. FTIR spectroscopic study of aniline polymerisation," *Synthetic metals,* vol. 154, pp. 1-4, 2005.

[54] S. RK, B. Gangadhar, H. Basu, V. Manisha, and N. GRK, "Remediation of malathion contaminated soil using zero valent iron nano-particles," *American Journal of Analytical Chemistry,* vol. 2012, 2012.

[55] S. Chatterjee, S. K. Das, R. Chakravarty, A. Chakrabarti, S. Ghosh, and A. K. Guha, "Interaction of malathion, an organophosphorus pesticide with Rhizopus oryzae biomass," *Journal of Hazardous Materials,* vol. 174, pp. 47-53, 2010.

[56] A. E. Lidiya, R. V. J. Raja, Q. M. Ngo, and D. Vigneswaran, "Detecting hemoglobin content blood glucose using surface plasmon resonance in D-shaped photonic crystal fiber," *Optical Fiber Technology,* vol. 50, pp. 132-138, 2019.

[57] N. Paliwal and J. John, "Sensitivity comparison of LMR based fiber optic refractive index (RI) sensors coated with different materials: Theoretical study," in *Australian Conference on Optical Fibre Technology*, 2016, p. AM3C. 6.

[58] S. K. Fanourakis, S. Q. Barroga, R. A. Mathew, J. Peña-Bahamonde, S. M. Louie, J. V. D. Perez*, et al.*, "Use of polyaniline coating on magnetic MoO3 and its effects on material stability and visible-light photocatalysis of tetracycline," *Journal of Environmental Chemical Engineering,* vol. 10, p. 107635, 2022.

[59] S. Bai, Y. Zhao, J. Sun, Z. Tong, R. Luo, D. Li*, et al.*, "Preparation of conducting films based on α-MoO3/PANI hybrids and their sensing properties to triethylamine at room temperature," *Sensors and Actuators B: Chemical,* vol. 239, pp. 131-138, 2017.

[60] H. A. Azab, A. S. Orabi, and A. M. Abbas, "New probe for fluorescence detection of Azinphous ethyl, Malathion and Heptachlor pesticides," *Journal of Luminescence,* vol. 160, pp. 181-187, 2015.

[61] W. Guo, B. J. Engelman, T. L. Haywood, N. B. Blok, D. S. Beaudoin, and S. O. Obare, "Dual fluorescence and electrochemical detection of the organophosphorus pesticides—ethion, malathion and fenthion," *Talanta,* vol. 87, pp. 276-283, 2011.

[62] F. Barahona, C. L. Bardliving, A. Phifer, J. G. Bruno, and C. A. Batt, "An aptasensor based on polymer-gold nanoparticle composite microspheres for the detection of malathion using surface-enhanced raman spectroscopy," *Industrial Biotechnology,* vol. 9, pp. 42-50, 2013.

[63] D. N. Kumar, A. Rajeshwari, S. Alex, M. Sahu, A. Raichur, N. Chandrasekaran*, et al.*, "Developing acetylcholinesterase-based inhibition assay by modulated synthesis of silver nanoparticles: applications for sensing of organophosphorus pesticides," *RSC advances,* vol. 5, pp. 61998-62006, 2015.

[64] D. Du, X. Ye, J. Cai, J. Liu, and A. Zhang, "Acetylcholinesterase biosensor design based on carbon nanotube-encapsulated polypyrrole and polyaniline copolymer for amperometric detection of organophosphates," *Biosensors and Bioelectronics,* vol. 25, pp. 2503-2508, 2010.

Graphical abstract: